Intern rapport ; IR 2008-03

Detection of Equatorial Waves using the Ozone Monitoring Instrument

I.R. van der Velde

De Bilt, 2008

KNMI Internal Report = Intern rapport ;IR 2008-03

De Bilt, 2008

PO Box 201
3730 AE De Bilt
Wilhelminalaan 10
De Bilt
The Netherlands
http://www.knmi.nl
Telephone +31(0)30-220 69 11
Telefax +31(0)30-221 04 07

Author: Velde, I.R. van der

Detection of Equatorial Waves using the Ozone Monitoring Instrument

M.Sc.-Internship

This report describes the research carried out during my stay at KNMI in the period between November 2007 and March 2008.

Author:
I. R. van der Velde, B.Sc.

Internship supervisors:
Dr. R. J. van der A
Prof. Dr. H. M. Kelder
Dr. W. T. M. Verkleij
KNMI, Royal Netherlands Meteorological Institute

Study supervisor:
Dr. L. J. M. Kroon
Meteorology and Air Quality Group, Wageningen University

April, 2008
De Bilt

Contents

Abstract

This report investigates the detection of equatorial waves, using satellite measurements from the Ozone Monitoring Instrument (OMI). These waves are rather interesting as they play an important role in the dynamics around the tropics and generate wave-like patterns in the stratospheric ozone concentration. To determine these dominant periodic signatures in the ozone concentration, the data is analyzed with a method of spectral analysis. By means of a linear model, we investigate if these signals can be attributed to equatorial waves.

We have obtained clear evidence that the eastward propagating signatures in 2005 and 2007 are in fact equatorial Kelvin waves. These signatures exhibit maximum amplitudes at the equator and correlate nicely with periods of westward zonal winds in the stratosphere. The signatures with planetary wave number 1 have periods about 12 to 15 days and it validates the findings of an earlier study, which used the contemporary GOME-instrument. Since OMI has a higher resolution in space and time, more Kelvin wave activity is detected with OMI. Additionally, we have also observed a Kelvin wave with wave number 2.

Furthermore, we have detected westward signatures in the northern and southern hemisphere during a period of predominantly westward winds. These signatures might indicate the presence of a mixed Rossby-gravity wave and a slow Rossby wave. Unfortunately, our simplified linear model and the correlations between ozone anomalies do not provide clear evidence.

1 Introduction

The dynamics of the equatorial region are rather different from the higher latitudes since the Coriolis force is small at the equator. As a consequence a unique dynamic region is established around the equator where trapped waves exist with unusually strong signals (Holton, 1992). Previous studies suggested that such waves are involved in atmospheric and oceanic phenomena such as the quasi-biennial oscillation (Holton and Lindzen, 1968), El Niño (Kessler and McPhaden, 1995), and phenomena that are associated with convection (Wheeler et al., 2000). Equatorial waves induce fluctuations of quantities like air pressure, wind, density and temperature. Investigations [e.g. Randel (1990); Randel and Gille (1991); Timmermans et al. (2004)] have demonstrated that equatorial Kelvin waves also induce fluctuations in the atmospheric constituents through advection or by changing the chemical processes (Feng et al., 2007). In the upper stratosphere, ozone has a short chemical lifetime and maintains a temperature dependent equilibrium of the concentrations through photochemical reactions. However, in the lower atmosphere, where ozone has a strong vertical gradient and a long photochemical lifetime, fluctuations are induced by motions (Timmermans et al., 2004).

This report is devoted to investigate equatorial wave signatures using satellite measurements from the Ozone Monitoring Instrument (OMI). By means of spectral analysis we will determine which of the wave numbers and frequencies are most dominant. Using linear theory, we investigate if these signals can be attributed to equatorial waves. Timmermans et al. (2004) conducted successfully a similar experiment to detect equatorial Kelvin waves using ozone column data from the Global Ozone Monitoring Experiment (GOME). With our study we expect first to validate the findings of Timmermans et al. (2004) and others, i.e. to confirm the possibility that Kelvin waves can be detected from ozone measurements. However, because OMI has a higher resolution in space and time, we anticipate that Kelvin waves create stronger significant signals than those observed by GOME. Finally, we hope to detect other branches of equatorial waves. To our knowledge, so far only Kelvin waves are identified from satellite ozone measurements.

In the M.Sc.-thesis of Van der Velde (2008), equatorial waves are studied theoretically using a linearized barotropic model on an equatorial beta-plane, a setting that is first explored by Matsuno (1966).

The *equatorial Kelvin wave* is an eastward propagating nondispersive wave, which is of fundamental importance to stratospheric and oceanic dynamics (Kiladis and Wheeler, 1995) and is associated with tropical deep convection (Feng et al., 2007). Previous observational studies have shown that Kelvin waves have a typical planetary wave number $s = 1$ (where s is the number of waves encircling the earth) and periods in the range of 12 to 20 days (Holton, 1992). Timmermans et al. (2004) argue that Kelvin waves are mainly detected when the background motions are westward, i.e. Kelvin waves that head against the main background current. In that case, the eastward moving Kelvin waves can propagate upward into the middle and upper stratosphere where its eastward momentum is transferred to the background current. The transfer of eastward momentum to the westward current will eventually lead to a reversal of the wind direction.

The *equatorial mixed Rossby-gravity wave* or Yanai wave is a dispersive wave that propa-

gates either eastward or westward. At high frequencies it behaves like a fast eastward gravity wave, while for low frequencies it behaves like a slow westward Rossby wave (Gill, 1982). The existence of the westward branch has been confirmed in observational data from the stratosphere in the equatorial Pacific (Holton, 1992). The observed waves have a typical planetary wave number $s = 4$ with periods in the range of 4 to 5 days. These westward mixed Rossby-gravity waves penetrate the eastward current carrying westward momentum to upper stratosphere where it is transferred to the background current (Timmermans et al., 2004).

From the linear theory two other waves have been derived: the dispersive *equatorial Rossby wave* and the *equatorial gravity wave*. The latter one, together with the Kelvin and mixed Rossby-gravity waves, are believed to be responsible for driving the quasi-biennial oscillation (QBO) and semi-annual oscillation (SAO). A westward propagating branch of the gravity wave is identified by Takayabu (1995) with periods in the range of 1.5 to 2.5 days. In contrast to the well documented oceanic Rossby waves, there is less evidence for the existence of an atmospheric Rossby wave. However, Kiladis and Wheeler (1995) presented a study where they obtained proof for a westward equatorial Rossby wave with planetary wave number $s = 6$ and strong signatures around the 850- to 700-mbar levels.

As mentioned above, the equatorial wave signatures acquired from ozone measurements are under investigation. The linear theory, that predicts the existence of equatorial waves, is discussed briefly in Chapter 2. In Chapter 3, the basic characteristics and methodology of the OMI-instrument and spectral analysis are discussed. Subsequently in Chapter 4, the results of the spectral analysis are presented with the use of periodograms. Finally, Chapter 5 presents the conclusions from the obtained results.

2 Linear Theory of Equatorial Waves

In this chapter we study the linear theory that predicts the existence of equatorial waves. Later on in Chapter 4 we will use this theory to identify the observed periodic signatures. Previously, it has been demonstrated (Van der Velde, 2008) that a set of primitive linear equations can be reduced, assuming a background state of uniform potential temperature, to a set of equations that is analogous to the shallow-water equations. The shallow-water model contains a set of equations, which describes the flow below a horizontal free-moving interface. One of the important features is that the velocity of the flow is constant with height. Approximating the geometry by an equatorial beta-plane and assuming a background state of no motion, the shallow-water momentum and continuity equations acquire the following form:

$$\frac{\partial u}{\partial t} - \beta y v = -g\frac{\partial \eta}{\partial x}, \tag{2.1}$$

$$\frac{\partial v}{\partial t} + \beta y u = -g\frac{\partial \eta}{\partial y}, \tag{2.2}$$

$$\frac{\partial \eta}{\partial t} + H\left(\nabla_z \cdot \mathbf{v}\right) = 0, \tag{2.3}$$

where $\mathbf{v}$ represents the horizontal wind with zonal component u and meridional component v, η is the perturbation of height and is related to the perturbation of surface pressure ($p'_s = \rho_r g\eta$). The mean depth of the layer is determined by H. Because we investigate waves around the equator we can approximate the Coriolis parameter by βy ($\beta = 2.3 \times 10^{-11}$ $\mathrm{m^{-1}s^{-1}}$ where y is the meridional distance from the equator). We have shown (Van der Velde, 2008) that the perturbation of absolute temperature T can be expressed in terms of η, assuming that the potential temperature of the background state is constant with height:

$$T = \frac{g\eta}{c_p}, \tag{2.4}$$

where c_p is the specific heat of dry air at constant pressure (1004 $\mathrm{JK^{-1}kg^{-1}}$) and g is the gravitational accelaration (≈ 9.8 m $\mathrm{s^{-2}}$).

The Kelvin wave, with motions being everywhere parallel to the equator, is an equatorial wave of the simplest kind. Setting $v = 0$ and eliminating u by combining (2.1)-(2.2) gives

$$\beta y \frac{\partial \eta}{\partial x} = \frac{\partial^2 \eta}{\partial y \partial t}. \tag{2.5}$$

In a similar way u can be eliminated from (2.3), i.e.

$$\frac{\partial^2 \eta}{\partial t^2} - gH\frac{\partial^2 \eta}{\partial x^2} = 0. \tag{2.6}$$

The solution to equations (2.5) and (2.6) can be written in the form of a sinusoidal plane wave:

$$\eta(x, y, t) = \hat{\eta}(y)e^{i(kx-\omega t)}, \tag{2.7}$$

where $\hat{\eta}(y)$ is the amplitude of the height perturbations at distance y from the equator. A dispersion relationship of permitted Kelvin waves with angular wave frequencies ω and zonal wave numbers k is obtained after substituting (2.7) into (2.6), i.e.

$$\omega = kc, \tag{2.8}$$

where $c = \sqrt{gH}$ is the characterized phase speed. The dispersion relation is visualized in Figure 2.1 together with the other equatorial waves. Subsequently, after substituting (2.7) into (2.5) one obtains

$$\beta y k\hat{\eta} = -\omega\frac{\partial \hat{\eta}}{\partial y}, \tag{2.9}$$

which is an ordinary differential equation satisfied by

$$\hat{\eta}(y) = \hat{\eta}_0 e^{(-\beta k y^2/2\omega)} = \hat{\eta}_0 e^{(-\beta y^2/2c)}. \tag{2.10}$$

Here $\hat{\eta}_0$ is the amplitude at the equator. In order to let the amplitude decay away from the equator, c has to be positive. Therefore, Kelvin waves propagate eastward. Combining (2.2), (2.4), (2.7), and (2.10) gives us the solutions for u, η and T:

$$u = \frac{g}{c}\hat{\eta}_0 e^{(-\beta y^2/2c)}e^{i(kx-\omega t)}, \tag{2.11}$$

$$\eta = \hat{\eta}_0 e^{(-\beta y^2/2c)} e^{i(kx-\omega t)}, \tag{2.12}$$

$$T = \frac{g}{c_p}\hat{\eta}_0 e^{(-\beta y^2/2c)} e^{i(kx-\omega t)}. \tag{2.13}$$

We can observe from this simplified barotropic model that Kelvin waves can modulate e.g. the height field, the zonal wind velocity and the temperature. As mentioned in the Introduction, Kelvin waves also induce fluctuations in the concentration of ozone and other trace gases as a result of fluctuations in temperature that cause the destruction and production of ozone (Timmermans et al., 2004). The set of equations (2.11)-(2.13) is valid for a background zonal wind of $\bar{u} = 0$. However, the model becomes more realistic if $\bar{u}$ is taken to be nonzero and constant. In the dispersion relation ω is then replaced by an intrinsic frequency $\hat{\omega} = \omega - k\bar{u}$. The frequency $\hat{\omega}$ can be interpreted as the frequency sensed by an observer moving along with the medium (Gill, 1982). To test this simplified system with the observations, one can approximate a Kelvin wave by assuming the following typical values: a planetary wave number $s = ka = 1$ around the latitude circle (with earth radius $a = 6370$ km), $\hat{\eta}_0 = 30$ m, $c = 30$ ms^{-1} and $\bar{u} = -20$ ms^{-1} (Holton, 1992). Solving the solutions (2.11)-(2.13) and the dispersion relation (2.8) results in a wave period of 15 days and maximum amplitudes of $u = 10$ ms^{-1} and $T = 0.30$ K at the equator. Wallace and Kousky (1968) observed periods between 10 and 20 days and amplitudes of $u = 8$ ms^{-1} and $T = 3$ K. Despite the model's simplicity, the magnitudes of the frequency and u are rather good. The absence of a more complex vertical profile might be responsible for the difference between the approximated and observed temperature. Figure 2.2 shows the height and horizontal velocity anomalies of a Kelvin wave as given by the linear model.

Other equatorial waves for which $v \neq 0$ are discussed by Van der Velde (2008), using the shallow-water equations (2.1)-(2.3). After some algebra a differential equation for v alone is obtained:

$$\frac{\partial}{\partial t}\left(\nabla_z^2 v - \frac{1}{c^2}\frac{\partial^2 v}{\partial t^2} - \frac{\beta^2 y^2}{c^2} v\right) + \beta\frac{\partial v}{\partial x} = 0. \tag{2.14}$$

Looking for solutions of the form

$$v(x, y, t) = \hat{v}(y) e^{i(kx-\omega t)}, \tag{2.15}$$

and formulating a dimensionless y-coordinate as

$$\xi = \left(\frac{\beta}{c}\right)^{1/2} y, \tag{2.16}$$

gives an equation that has the same form as a quantum mechanical oscillator and is satisfied by an infinite set of equatorial waves:

$$\frac{\partial^2 \hat{v}}{\partial \xi^2} - \xi^2 \hat{v} + (2n+1)\,\hat{v} = 0, \tag{2.17}$$

The index $(2n + 1)$ satisfies the corresponding dispersion relation, which can be written in following form:

$$(2n+1)\frac{\beta}{c} = \frac{\omega^2}{c^2} - k^2 - \frac{\beta k}{\omega}, \tag{2.18}$$

The meridional structure of the equatorial waves is given by

$$\hat{v}_n(\xi) = \hat{v}_0 2^{-n/2} e^{-\xi^2/2} H_n(\xi), \tag{2.19}$$

where $c = \sqrt{gH}$ is the shallow-water phase speed, $H_n(\xi)$ represents an infinite set of Hermite polynomials of mode number $n = 0, 1, 2...$ and $\hat{v}_0$ is the amplitude of meridional velocity at the equator.

Only if $n = -1$, the dispersion relation (2.18) is exactly solved for a Kelvin wave. For $n = 0$ we have a somewhat special wave. It can behave like a fast gravity wave if k is large and positive or like a slow planetary wave if k is large and negative. For that reason it is called the mixed Rossby-gravity wave or the Yanai wave (Gill, 1982). The phase speed can either be east or west. Its dispersion relation yields

$$\frac{\omega}{c} - k - \frac{\beta}{\omega} = 0, \tag{2.20}$$

or as a function of k (Holton, 1992):

$$\omega = kc \left[\frac{1}{2} \pm \frac{1}{2} \left(1 + \frac{4\beta}{k^2 c} \right)^{1/2} \right], \tag{2.21}$$

where the plus-sign corresponds with an eastward propagating wave, while the minus-sign corresponds with a westward propagating wave. The dispersion relation is drawn in Figure 2.1 together with the other equatorial waves.

For $n \geq 1$, waves can be divided into two groups; the high-frequency gravity waves and low-frequency Rossby waves. For the high-frequency waves the dispersion relation can be approximated by neglecting term $\beta k/\omega$ in (2.18), i.e.

$$\omega^2 = c^2 k^2 + (2n+1)\beta c, \tag{2.22}$$

while the dispersion relation for the Rossby waves is approximated by neglecting ω^2/c^2, i.e.

$$\omega = \frac{-\beta k}{k^2 + (2n+1)\frac{\beta}{c}}. \tag{2.23}$$

As one can see in Figure 2.1, gravity waves may propagate eastward (for positive wave numbers) or westward (for negative wave numbers). Rossby waves on the other hand only propagate westward. Figure 2.2 shows the height and horizontal velocity anomalies of all equatorial waves.

As for the Kelvin waves, we can introduce an intrinsic frequency $\hat{\omega}$ if a background flow $\bar{u}$ is present.

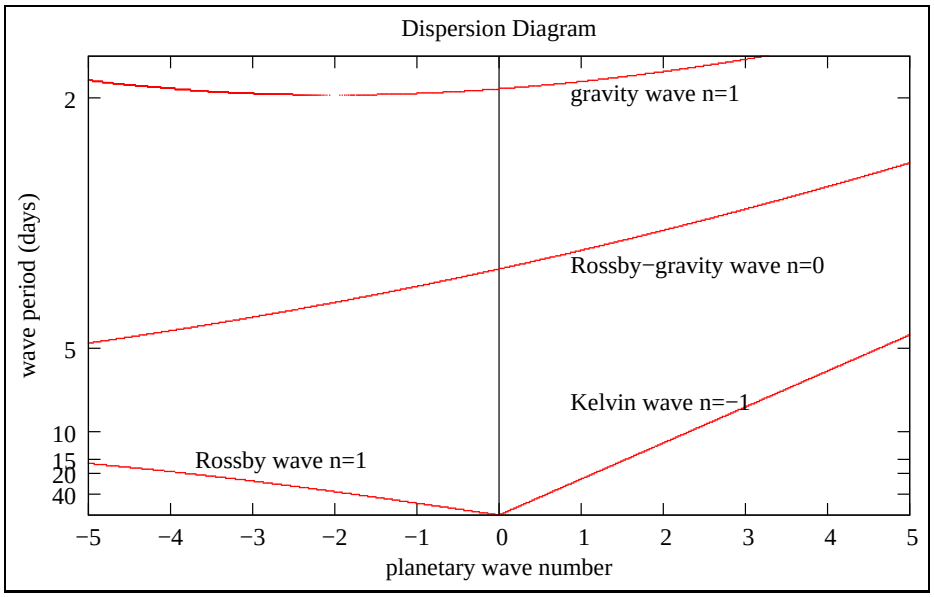

Figure 2.1: *Dispersion diagram for equatorially trapped waves in case of $\bar{u}$ =0. The horizontal axis represents the planetary wave number $s = ka$, i.e. the number of waves encircling the earth. The vertical axis represents the wave period τ in units of days. It is simply solved by $\tau = \frac{2\pi}{\omega \cdot 86400}$, where ω is written as function of $s/a = k$. Westward traveling waves have negative wave numbers and eastward traveling waves have positive wave numbers. The equatorial Rossby and gravity waves are plotted for n=1, the mixed Rossby-gravity wave for n=0 and the Kelvin wave for n=-1.*

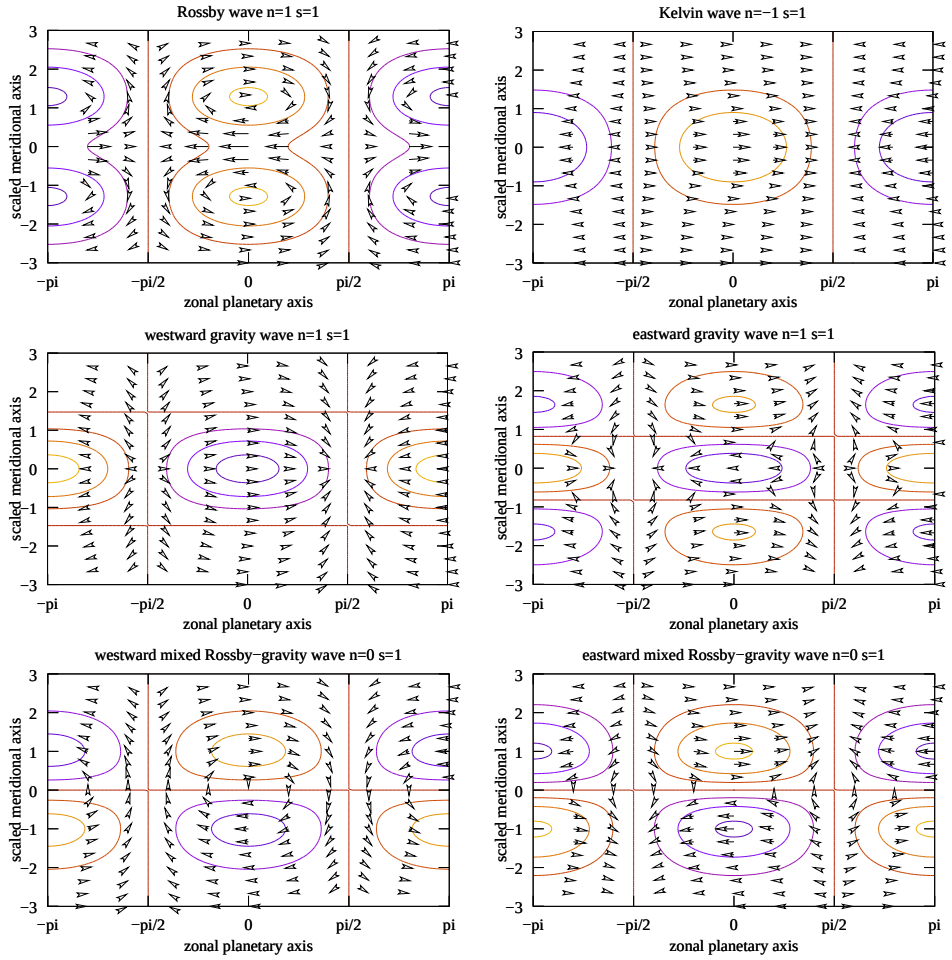

Figure 2.2: *The height and horizontal velocity anomalies for all four equatorial waves for wave number s=1. Positive height anomalies have an orange color and the negative height anomalies a blue color. The Rossby and the gravity wave are simulated for n=1.*

3 Data and Methodology

Our main goal in this study is the detection of periodic signals in ozone measurements. The current chapter illustrates how the ozone data is obtained and it also describes a commonly used technique in spectral analysis: the periodogram.

The Ozone Monitoring Instrument (OMI) flies on board NASA's EOS-Aura satellite, which was launched on 15 July 2004. It is built by Dutch Space and TNO Science & Industry. OMI is a nadir viewing imaging spectrometer that measures the solar radiation scattered by the earth's atmosphere and surface over a wavelength range from 264 to 504 nm. It enables us to retrieve the concentrations of different trace gases in the atmosphere, e.g. ozone, nitrogendioxide, aerosols and other constituents. The telescope has a viewing angle of 114^o, which covers a spatial area of 13 km in latitudinal and 2600 km in longitudinal direction. An advantage of OMI is the ability to do measurements with a daily global coverage. In comparison to the GOME-instrument, where global coverage is only reached

after three days.

Our study is based on level 3 total ozone column data. The measured values are processed using the DOAS algorithm version 3 (Differential Optical Absorption Spectroscopy) and are laid on a grid with a spatial resolution of 0.25^o x 0.25^o. Furthermore, measurements with the highest uncertainty, e.g. at the edges of the viewing area, are filtered out to keep only the best values. Ozone concentration under complete cloud cover cannot be determined by OMI and is therefore derived from the climatology.

The total ozone columns are validated with Brewer measurements for the Northern hemisphere, for November 2004 as for the period between 28 March and 11 June 2005. On average, the retrieved ozone column is biased by 2 % (from the OMDOAO3 README document).

The data used for this study covers the period between December 2004 and January 2008. Ozone observations are collected on latitude-longitude gridcells of 2.5^o x 2.5^o. The grid cells are placed along three different latitude bands: one around the equator, between 1.25^o S and 1.25^o N, one between 8.75^o N and 11.25^o N and one between 8.75^o S and 11.25^o S. Analyzing Figure 2.2, one can expect the highest equatorial wave amplitudes around these latitude circles. Within each grid cell measurements are averaged to obtain a single value per grid cell. The grid size of 2.5^o x 2.5^o is chosen because it led to a 2 times better spatial resolution compared to the GOME study and still it maintained a rather short computation time. Since the data is processed on a 0.25^o x 0.25^o grid, a maximum of 100 measurements are available per grid cell. Unfortunately, for some of the grid cells no average value is obtained because the data contained gaps. A special method in spectral analysis allows us to investigate such unevenly spaced data.

Spectral analysis is based on the discrete Fourier transform, where a function in terms of time is transformed into a function in terms of frequency. Its theoretical and practical usage is discussed by Scargle (1982). As a simple example, the Fourier transform for a data set $\chi(t_j), j = 1, 2, ..., N$ yields

$$FT(\omega) = \sum_{j=1}^{N} \chi(t_j) e^{-i\omega t_j}.$$

A classical periodogram, as a function of frequency ω is then given by

$$P(\omega) = \frac{1}{N} \mid \sum_{j=1}^{N} \chi(t_j) e^{-i\omega t_j} \mid^2,$$

or

$$P(\omega) = \frac{1}{N} \left[\left(\sum_{j=1}^{N} \chi(t_j) \cos \omega t_j \right)^2 + \left(\sum_{j=1}^{N} \chi(t_j) \sin \omega t_j \right)^2 \right]. \tag{3.1}$$

If χ has a sinusoidal component with frequency ω_0, then near $\omega = \omega_0$, χ and $exp(-i\omega t)$ are in phase and make a large contribution to the sums in equation (3.1). For any other value of ω the terms in the sums are randomly positive and negative which yields a small outcome. Hence, the presence of a sinusoidal signal creates a peak in the spectrum. For

evenly sampled data, i.e. when the time between each measurement is constant, it is rather easy to determine the significance of the spectral peaks. However, if the data is unevenly spaced, the statistical distribution is much more complicated (Timmermans et al., 2004). The inconvenient fact is that our satellite data has two dimensions (time and space) and is unevenly spaced for both of them. To deal with this problem we might use the technique of interpolation. It is argued though that such techniques perform poorly. Long gaps in the data often produce spurious power signals at low frequencies at wavelengths comparable to the gaps [Timmermans et al. (2004); Press et al. (1992)].

Lomb developed a modified version of the classical periodogram that retains a simple statistical behavior, even for unevenly spaced data. The Lomb-method, discussed in detail by Press et al. (1992) and Scargle (1982), evaluates the data at the actual measured locations and times. Because we deal with data in space and time we use the two-dimensional version of the Lomb-periodogram derived by Timmermans et al. (2004). For each of the three latitude bands we obtain a data set with total data points N_{tot} and ozone values $\chi(t_j, x_l)$. These values are measured at days t_j, with $j = 1, 2, ..., N_t$, and longitude locations x_l, with $l = 1, 2, ..., N_x$. The normalized Lomb-periodogram as a function of wave number k and angular frequency ω takes the following form:

$$\begin{aligned} P_{Lomb}(\omega, k) &= \frac{1}{2\sigma^2}\left[\frac{\left(\sum_{j,l}(\chi(t_j,x_l)-\bar{\chi})\cos\left(\omega(t_j-\tau_1)\pm k(x_l-\tau_2)\right)\right)^2}{\sum_{j,l}\cos^2\left(\omega(t_j-\tau_1)\pm k(x_l-\tau_2)\right)}\right] \\ &\quad + \frac{1}{2\sigma^2}\left[\frac{\left(\sum_{j,l}(\chi(t_j,x_l)-\bar{\chi})\sin\left(\omega(t_j-\tau_1)\pm k(x_l-\tau_2)\right)\right)^2}{\sum_{j,l}\sin^2\left(\omega(t_j-\tau_1)\pm k(x_l-\tau_2)\right)}\right], \end{aligned} \tag{3.2}$$

with constants

$$\tau_1 = \frac{1}{2\omega} atan\left[\frac{\sum_j \sin 2\omega t_j}{\sum_j \cos 2\omega t_j}\right], \tag{3.3}$$

$$\tau_2 = \frac{1}{2k} atan\left[\frac{\sum_l \sin 2k x_j}{\sum_l \cos 2k x_l}\right], \tag{3.4}$$

mean ozone value

$$\bar{\chi} = \frac{1}{N_{tot}} \sum_{j=1}^{N_t}\sum_{l=1}^{N_x} \chi(t_j, x_l), \tag{3.5}$$

and the normalize factor

$$\sigma^2 = \frac{1}{N_{tot}-1} \sum_{j=1}^{N_t}\sum_{l=1}^{N_x} \left(\chi(t_j,x_l)-\bar{\chi}\right)^2. \tag{3.6}$$

The eastward propagating signatures are calculated with a minus-sign and the westward propagating signatures with a plus-sign.

Press et al. (1992) and Scargle (1982) show us that choosing the constants τ_1 and τ_2 will make (3.2) equivalent to the equation that one would obtain if an harmonic data set is estimated by least-squares fitting. The major advantages of the Lomb-method are that it handles unevenly spaced data and it enables evaluation of its statistical behavior.

Often a data set is a sum of independent Gaussian noise and periodic signals. The noise may create spectral peaks in P_{Lomb} and are erroneously identified as periodic signals. Therefore, it is important to analyze the significance of spectral peaks by asking ourselves the question: 'what is the probability that a peak in P_{Lomb} is caused by random noise?' A null hypothesis H_0 is formulated, which assumes χ is only pure independent Gaussian noise. Since P_{Lomb} is normalized it supposes in the case of H_0 an exponential distribution with a mean. The probability that P_{Lomb} lies between z and $z + dz$ is given by

$$p_r\left(z < P_{Lomb} < z + dz\right) = e^{-z}dz.$$

If M amount of independent frequencies are sampled, then the probability that P_{Lomb} gives values not higher than z is

$$p_r\left(P_{Lomb} \leqslant z\right) = \left(1 - e^{-z}\right)^M.$$

Thus the probability that P_{Lomb} gives values higher than z is simply

$$p_0 = p_r\left(P_{Lomb} > z\right) = 1 - \left(1 - e^{-z}\right)^M, \tag{3.7}$$

which is the false-alarm probability of the H_0 hypothesis. If the false-alarm probability p_0 is small, then a periodic signal becomes more significant. It is desirable to find threshold level z_0 for which a probability p_0 exists the signal is caused by noise. The expression for z_0 follows from 3.7 (Scargle, 1982):

$$z_0 = -\ln\left[1 - (1 - p_0)^{1/M}\right]. \tag{3.8}$$

If $p_0 = 0.01$, the periodic signal is 99 % significant when a signal is exceeding the z_0-level.

To calculate the number of independent frequencies M we use the definition

$$M = -6.362 + 1.193N_{tot} + 0.00098N_{tot}^2, \tag{3.9}$$

which is determined by Horne and Baliunas (1986).

4 Results

Before the periodic signatures are scrutinized we take a closer look at the zonal mean wind $\bar{u}$ in the stratosphere. The direction of $\bar{u}$ is an important factor to detect equatorial waves. For example, a Kelvin wave is most easily detected in the presence of a westward zonal wind, i.e. a flow in the opposite direction of the phase propagation. Figure 4.1 presents the NCEP monthly mean values of $\bar{u}$ around the equatorial latitude circle at 30 hPa. Between December 2004 and January 2008 periodic reversals of $\bar{u}$ are clearly visible and are related to the quasi-biennial oscillation. There are two distinct periods of $\bar{u} < 0$ and one period of $\bar{u} > 0$.

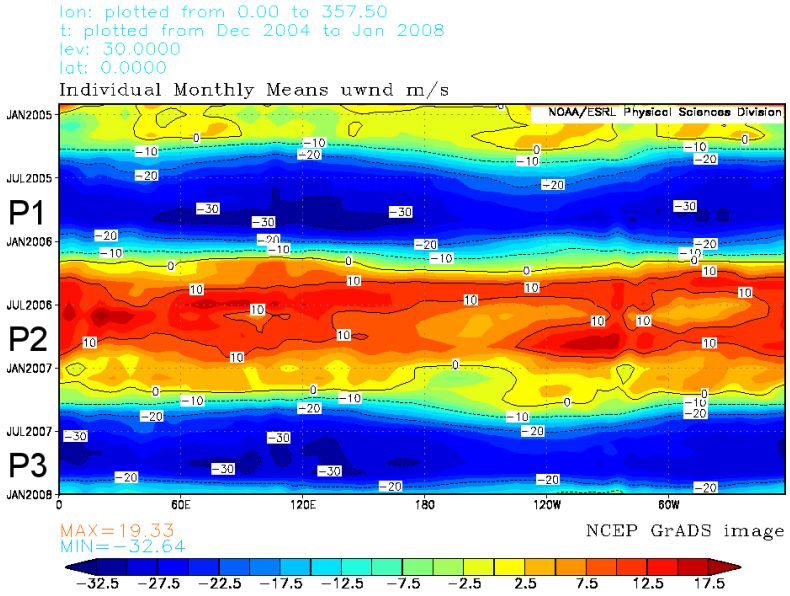

Figure 4.1: *The monthly mean zonal wind at 30 hPa around the equatorial latitude circle between December 2004 and January 2008. The symbols P1, P2 and P3 point to periods, which are investigated by the Lomb-method. ["Image provided by the NOAA-ESRL Physical Sciences Division, Boulder Colorado from their Web site at http://www.cdc.noaa.gov/".]*

To calculate the Lomb-periodograms, a period of $N_t = 60$ days is chosen. According to Timmermans et al. (2004) and Feng et al. (2007), a 60-day period is appropriate to study Kelvin wave signals. The ozone values are averaged on a fixed 2.5^o x 2.5^o grid, therefore, for each latitude band we have obtained $N_x = 144$ grid cells. Additionally, the 90%, 99% and 99.9% significant levels are determined with expression (3.8) and correspond respectively to the colors blue, green and red in the Lomb-periodograms.

Figure 4.2 presents the Lomb-periodograms for the period between 29 July and 26 September 2005 ($P1$; see Figure 4.1). The periodogram on the left is made for the latitude circle at 10^o S, the one in the middle is made for the equator and the one on the right is

made for 10^o N. At each latitude circle we observe a clear significant eastward propagating signal with a 15-day period and a planetary wave number $s = 1$. It agrees with typical shallow-water Kelvin wave characteristics. Furthermore, the signatures in the northern and southern hemisphere are weaker than at the equator.

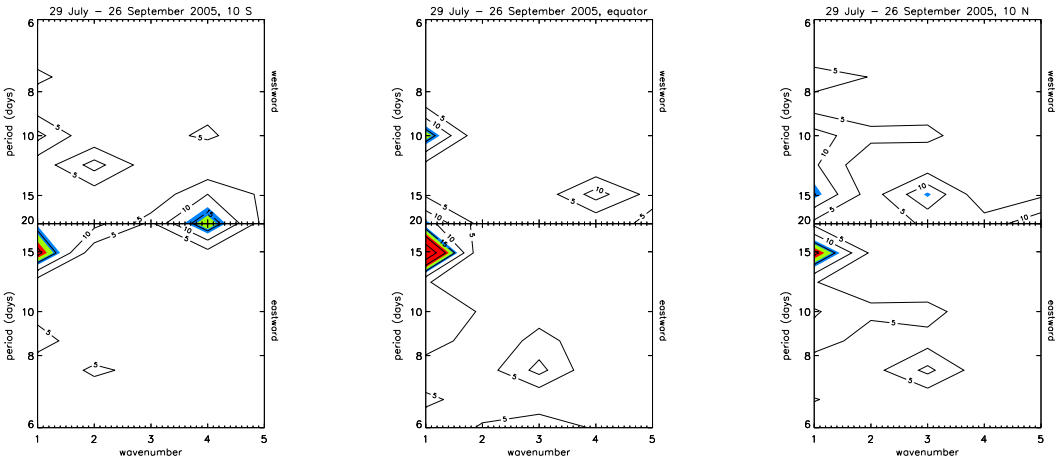

Figure 4.2: *Lomb-periodograms for the period between 29 July and 26 September 2005 (P1). The periodogram on the left is made for 10^o S, the one in the middle is made for the equator and the one on the right is made for 10^o N. The x-axis represents the planetary wave number and the y-axis represents the wave period in the range between 6 and 20 days. The upper part detects the westward wave signatures and the lower part detects the eastward signatures. The colors blue, green and red correspond respectively with the 90%, 99% and 99.9% significant levels.*

The second period of interest, between 25 August and 23 October 2006 ($P2$; see Figure 4.1), is characterized by predominantly eastward zonal winds. Figure 4.3 shows for that period the Lomb-periodograms at the three latitude bands. No significant signatures are visible that can be related to any of the equatorial waves. This outcome is expected for Kelvin waves, since the presence of an eastward zonal wind is not favorable for detection (Timmermans et al., 2004). For the mixed Rossby-gravity waves, we might expect signals in the westward branch. Wave periods of approximately 3 days are predicted with the shallow-water theory. However, such signals are not detected.

In the last 60-day period, between 12 June and 10 August 2007 ($P3$; see Figure 4.1), the zonal wind is westward again, akin to $P1$. Figure 4.4 reveals several interesting signatures that propagate east- and westward. The two significant signatures in the eastward branch correspond to planetary wave numbers 1 and 2 and periods around 12 and 7 days. The peaks are denoted with $E1$ and $E2$. Weaker signals of $E1$ are also observed at the northern and southern hemisphere. Yet, a weaker signal of $E2$ is only seen at the northern hemisphere. The eastward signals strongly suggest the presence of Kelvin waves. It can be proven by characterizing two Kelvin waves with wave numbers 1 and 2, using the Kelvin wave dispersion relation (2.8) and taking a westward wind into account. Investigating the processed artificial

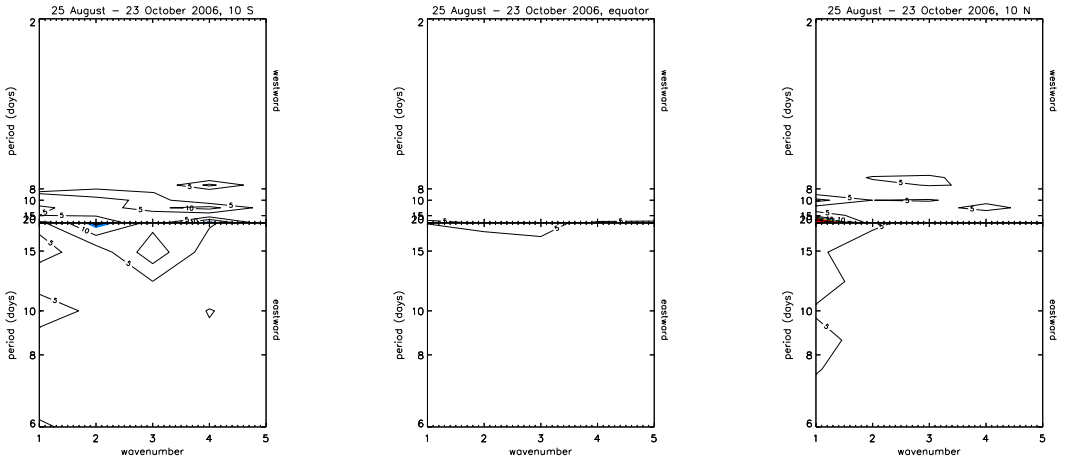

Figure 4.3: *Lomb-periodograms for the period between 25 August and 23 October 2006 (P2). The y-axis of the westward branch is now chosen between 2 and 20 days. The other properties are the same as for Figure 4.2.*

data reveals signatures that are analogous to the observations, as it is demonstrated by the fourth periodogram in Figure 4.4.

The westward branch shows signatures in the northern and southern hemisphere. Two distinct peaks are visible: a cluster of slow periodic signals with periods around 10 to 20 days ($W1$) and a faster signal with a period around 7 days ($W2$). The detection is quite remarkable since the zonal wind travels in the same direction as the wave propagation. Because there are no clear peaks observed at the equator, this suggests a westward mixed Rossby-gravity wave or a slow Rossby wave. As the shallow-water model predicts, their maximum height amplitudes are away from the equator (see Figure 2.2). The model predicts wave periods of around three days for the mixed Rossby-gravity wave, which is slower than the observed $W2$ signal. Yet, for a Rossby wave the model predicts under the current conditions (i.e. a westward mean wind) a wave period of 20 days and agrees fairly with the observed $W1$ signal (see the fifth periodogram in Figure 4.4).

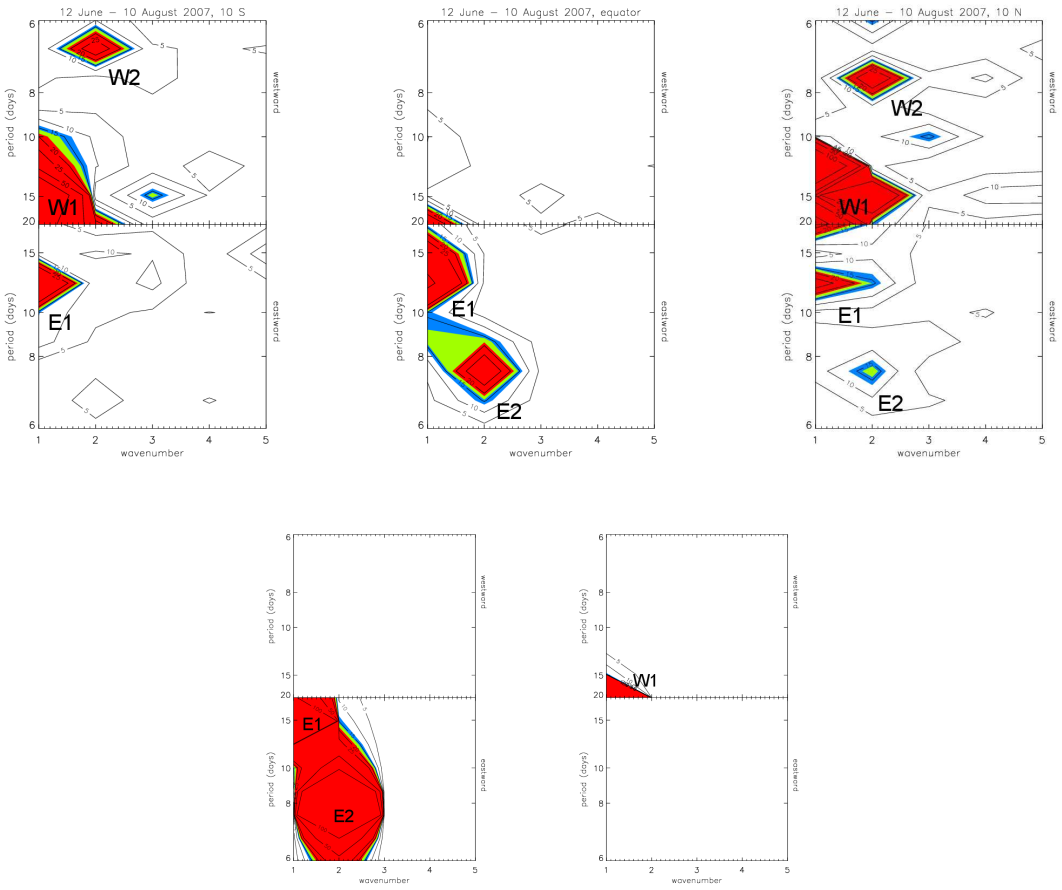

Figure 4.4: *Lomb-periodograms for the period between 12 June and 10 August 2007 (P3). The properties of the first three diagrams are the same as for Figure 4.2. The fourth periodogram shows the spectral power of artificial Kelvin signals, characterized by the Kelvin wave dispersion relation (2.8). Finally, the fifth periodogram shows the spectral power of an artificial Rossby signal, characterized by (2.18). The symbols E1, E2, W1 and W2 point to the significant east- and westward signatures.*

As it is revealed by Figure 2.2, the height anomalies between hemispheres are either positively or negatively correlated. For the Kelvin and Rossby waves the correlation is positive, while for the mixed Rossby-gravity wave the correlation is negative. A similar correlation is expected for ozone fluctuations. Determining the correlation coefficient between both hemispheres might offer additional evidence that the observed signatures are associated with equatorial waves. A filter is used to extract ozone values at the significant wave periods and wave numbers. All observed eastward signatures in $P1$ and $P3$ are positively correlated in the range between 0.8 and 0.95. It gives additional evidence the signatures are indeed induced by Kelvin waves. Unfortunately, the westward signatures in $P3$ give quite ambiguous results. The fast signal $W2$ gives a correlation of -0.2, while $W1$ is correlated in the range of 0.3-0.4.

Figure 4.5 shows time versus longitude plots (Hovmöller diagrams) of the prominent eastward signature $E1$. Again it reveals typical characteristics that correspond with Kelvin waves. It travels eastward with a phase speed that varies around 20-40 ms^{-1}. The strongest amplitudes are observed at the equator.

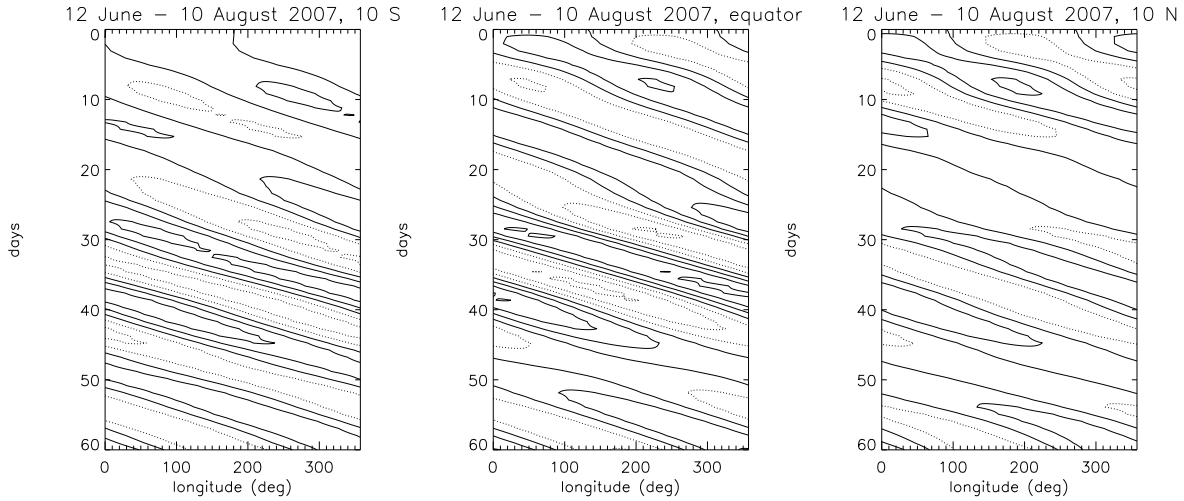

Figure 4.5: *Ozone Hovmöller diagrams for signature E1 in the period P3. The diagram on the left is made for 10º S, the one in the middle is made for the equator and the one on the right is made for 10º N. The x-axis represents the longitudinal position in unit degrees and the y-axis represents the 60-day time period. The solid lines correspond with positive ozone anomalies and the dashed lines correspond with negative anomalies. The contour lines are drawn with an interval of 0.5 DU*

Episodes of Kelvin wave activity in the period 2005-2008 are plotted in Figure 4.6. It presents two time series: one for planetary wave number 1 with 12- and 15-day wave periods, and one for planetary wave number 2 with 8- and 10-day wave periods. The 99.9% significance level is set at 18. For wave number 1 several significant episodes are observed in periods $P1$ and $P3$. The largest signatures, with a maximum spectral power at 80, are observed in the summer of 2007. As anticipated, there is not much activity in period $P2$. For wave number 2 clear signals are detected in period $P3$, and correspond to wave $E2$. Timmermans et al. (2004) identified, in the period 1995-2002, only three occasions of high Kelvin wave activity. These signatures had a spectral power around 30-40 and a 99.9% significance level at 14. Apparently, OMI is able to detect more significant Kelvin wave activity than GOME.

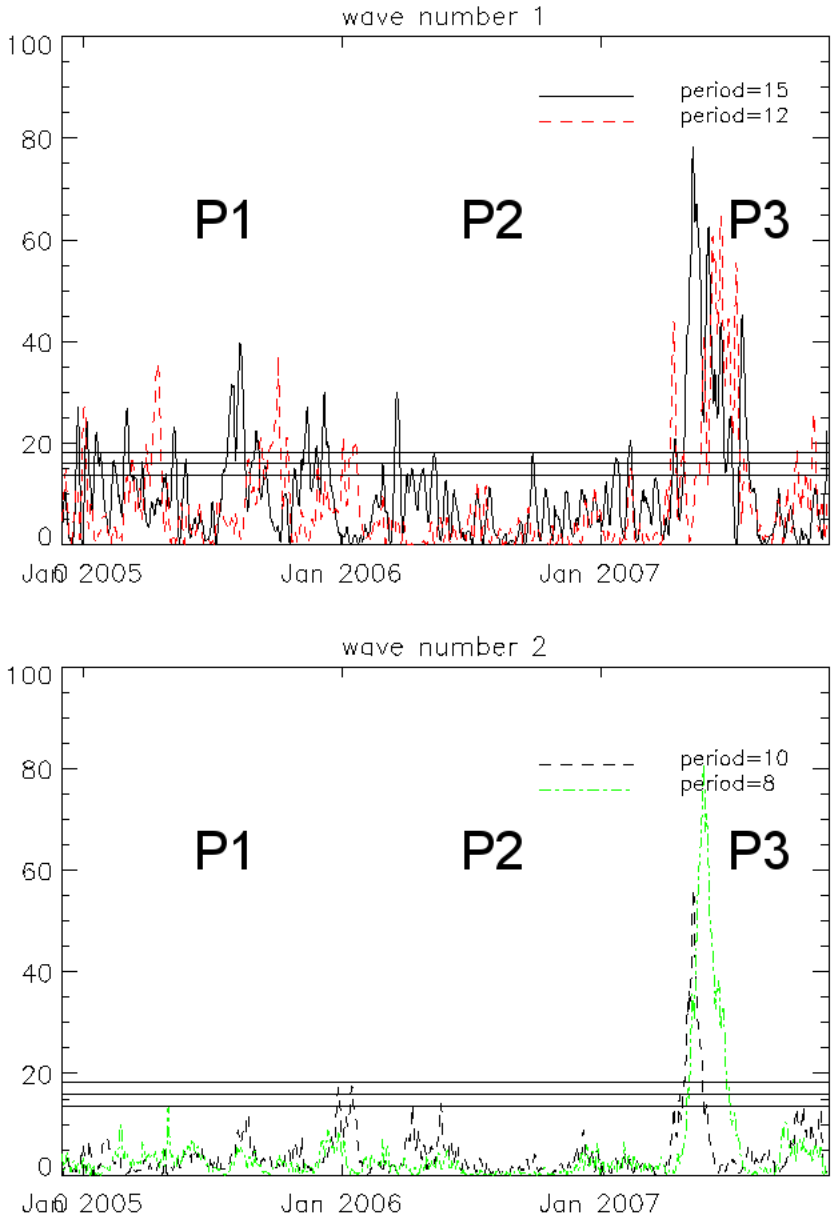

Figure 4.6: *Lomb-periodogram time serie plots for a three year period. The upper plot shows wave number 1 at a 12- and 15-day period, while the lower plot shows wave number 2 at a 8- and 10-day period. The symbols P1, P2 and P3 indicate the periods that are analyzed. The 90%, 99% and 99.9% significance levels are drawn by horizontal lines.*

5 Conclusions and Discussion

In this Internship-report the detection of equatorial waves has been studied using the Ozone Monitoring Instrument (OMI). Equatorial waves are rather interesting as they modulate the stratospheric ozone concentration by temperature-dependent chemical processes and vertical

advection. The observed ozone data has been investigated with a special method of spectral analysis to determine the dominant periodic signatures. We have used the so-called Lomb-method because it allows examination of unevenly spaced data and it provides a way to assess the statistical significance. To identify the periodic signatures, a single-layer linear model is used to calculate the various equatorial waves.

We have obtained evidence that the eastward propagating signatures in 2005 and 2007 are in fact equatorial Kelvin waves. These signatures exhibit maximum amplitudes at the equator and correlate nicely with periods of westward zonal winds in the stratosphere. The signatures with planetary wave number 1 have periods about 12 to 15 days. The observed features are in agreement with typical Kelvin wave characteristics. It validates the findings of Timmermans et al. (2004), who performed a similar kind of study with GOME. On one occasion we also observed Kelvin wave signatures with wave number 2.

We can conclude that OMI is able to detect more Kelvin wave activity than GOME. First of all, we have used a higher resolution in space and secondly, OMI is sampling the ozon concentration with global coverage every day. In comparison, GOME needs three days to reach global coverage.

In addition, we have detected westward signatures in the northern and southern hemisphere during a period of predominantly westward winds. These signatures indicate the presence of a mixed Rossby-gravity wave and a slow Rossby wave. Unfortunately, our simplified linear model and the correlations between ozone anomalies do not provide clear evidence. It is obvious that more study is needed to identify the westward signatures.

Finally, in comparison to 2005, we observed in 2007 stronger spectral power of Kelvin wave activity. The main reason for this difference remains unclear and more research is desirable.

References

Feng, L., R. S. Harwood, R. Brugge, A. O'Neill, L. Froidevaux, M. Schwartz, and J. W. Waters, 2007: Equatorial kelvin waves as revealed by eos microwave limb sounder observations and european centre for medium-range weather forecasts analyses: Evidence for slow kelvin waves of zonal wave number 3. *J. Geophys. Res.*, **112**, doi:10.1029/2006JD008329.

Gill, A. E., 1982: *Atmosphere-Ocean Dynamics*. Academic Press, San Diego.

Holton, J. R., 1992: *An Introduction to Dynamic Meteorology*. Academic Press, San Diego, third edition.

Holton, J. R. and R. S. Lindzen, 1968: A note on kelvin waves in the atmosphere. *Mon. Weather Rev.*, **96**, 385–386.

Horne, J. H. and S. L. Baliunas, 1986: A prescription for period analysis of unevenly sampled time series. *Astrophys. J.*, **302**, 451–465.

Kessler, W. S. and M. J. McPhaden, 1995: Oceanic equatorial waves and the 1991-93 el nino. *J. Climate*, **8**, 1757–1774.

Kiladis, G. N. and M. Wheeler, 1995: Horizontal and vertical structure of observed tropospheric equatorial rossby waves. *J. Geophys. Res.*, **100**, 22981–22997.

Matsuno, T., 1966: Quasi-geostrophic motions in the equatorial area. *J. Meteorol. Soc. Japan*, **44**, 25–43.

Press, W. H., B. P. Flannery, S. A. Teukolsky, and W. T. Vetterling, 1992: *Numerical Recipes in FORTRAN: The Art of Scientific Computing*. Cambridge University Press, New York, second edition.

Randel, W. J., 1990: Kelvin wave-induced trace constituent oscillations in the equatorial stratosphere. *J. Geophys. Res.*, **95**, 18641–18652.

Randel, W. J. and J. C. Gille, 1991: Kelvin wave variability in the upper stratosphere observed in sbuv ozone data. *J. Atmos. Sci.*, **48**, 2336–2349.

Scargle, J. D., 1982: Studies in astronomical time series analysis. ii - statistical aspects of spectral analysis of unevenly spaced data. *Astrophys. J.*, **263**, 835–853.

Takayabu, Y. N., 1995: Large-scale cloud disturbances associated with equatorial waves. part ii: Westward-propagating inertio-gravity waves. *J. Meteorol. Soc. Japan*, **72**, 451–465.

Timmermans, R. M. A., R. F. van Oss, and H. M. Kelder, 2004: Equatorial kelvin wave signatures in ozone column measurements from gome. *J. Geophys. Res.*, **109**, doi:10.1029/2003JD003946.

Van der Velde, I. R., 2008: *Study of Geostrophic Waves around the Equator*. Master's thesis, KNMI; Wageningen University.

Wallace, J. M. and V. E. Kousky, 1968: Observational evidence of kelvin waves in the tropical stratosphere. *J. Atmos. Sci.*, **25**, 900–907.

Wheeler, M., G. N. Kiladis, and P. J. Webster, 2000: Large-scale dynamical fields associated with convectively coupled equatorial waves. *J. Atmos. Sci.*, **57**, 613–640.

Acknowledgments

My study at KNMI has been generously supported by Ronald van der A, Henny Kelder, Wim Verkleij and Renske Timmermans. I would like to thank particularly these people for there assistance and encouragement to finish my thesis. I thank the people at Weer-Onderzoek who gave me a workspace. Furthermore, I am grateful to my study supervisor Leo Kroon, my family, friends and my love Magdalena for their support.